

Effects of finite temperature and pairing correlations in multi- Λ hypernucleiBahruz Suleymanli *Physics Department, Yildiz Technical University, 34220 Esenler, Istanbul, Turkey*Kutsal Bozkurt *Physics Department, Yildiz Technical University, 34220 Esenler, Istanbul, Turkey
and Université Paris-Saclay, CNRS/IN2P3, IJCLab, 91405 Orsay, France*Elias Khan *Université Paris-Saclay, CNRS/IN2P3, IJCLab, 91405 Orsay, France
and Institut Universitaire de France (IUF)*Haşim Güven *Université Paris-Saclay, CNRS/IN2P3, IJCLab, 91405 Orsay, France
and Physics Department, Yildiz Technical University, 34220 Esenler, Istanbul, Turkey*

Jérôme Margueron

*Université Lyon, Université Claude Bernard Lyon 1, CNRS/IN2P3, IP2I Lyon, UMR 5822, F-69622 Villeurbanne, France
and International Research Laboratory on Nuclear Physics and Astrophysics,
Michigan State University and CNRS, East Lansing, Michigan 48824, USA*

(Received 18 March 2024; revised 31 May 2024; accepted 11 July 2024; published 26 July 2024)

The influence of finite temperatures and pairing correlations on the ground-state properties of multi- Λ Ca, Sn, and Pb hypernuclei is explored using the finite-temperature Hartree-Fock-Bogoliubov approach and contact pairing interaction. A critical temperature is predicted and is in agreement with the Bardeen-Cooper-Schrieffer relationship $k_B T_C^\Lambda \approx 0.5 \Delta_\Lambda^{T=0}$, beyond which pairing correlations drop to zero. Particle densities, Λ single-particle energies, and nuclear radii are weakly impacted by pairing as well as by finite temperatures. However, other nuclear properties which are more sensitive to pairing correlations, such as Λ -pairing gaps, condensation energies, and abnormal densities are also more impacted by finite temperature, especially around the critical temperature. Furthermore, calculations show the occurrence of the pairing re-entrance effect in the ${}_{70\Lambda}^{280}\text{Pb}$ hyperon drip-line hypernucleus. Our study provides insight into the thermal evolution of Λ pairing, i.e., the emergence and vanishing of pairing correlations in multi- Λ hypernuclei as a function of temperature.

DOI: [10.1103/PhysRevC.110.014329](https://doi.org/10.1103/PhysRevC.110.014329)**I. INTRODUCTION**

Including the temperature effect in nuclear systems can have a large impact on astrophysical processes [1]. Hot nuclear matter exists only temporarily in compact stars and in finite nuclei since thermal energy can be efficiently evacuated by neutrino and γ -ray emissions. The properties of hot matter may, however, be different from the ones of cold systems such as neutron stars (NSs) or finite nuclei and may influence time evolution. For instance, protoneutron stars (PNSs) are transient celestial objects for which temperature impacts dynamical evolution [2–5]. During the first few seconds after their formation by massive-star core collapse (supernovae) or by binary neutron star mergers (kilonovae), matter can be heated to temperatures of the order of a few 10^{11} K, which drops down to about $T \lesssim 10^{10}$ K in less than an hour [6]. During this cooling, hypernuclear matter may temporarily exist in hot PNSs [7,8], but the actual presence of hyperons

in the inner core of PNSs crucially depends on the hyperon-hyperon interaction [9]. Consequently, the interplay between the hyperon-hyperon interaction and temperature plays an important role in the understanding of the cooling properties of PNSs.

The uncertainties in the hyperon-hyperon interaction are, however, still too large to allow accurate predictions about hyperon matter. These uncertainties are largely due to the scarce amount of experimental data, since only a limited number of double- Λ hypernuclei, including ${}_{\Lambda\Lambda}^6\text{He}$ and ${}_{\Lambda\Lambda}^{11}\text{Be}$ [10–12] have been produced and measured in laboratories. In the future, the production of hyperons at FAIR and JPARC will provide new data which will be employed to reduce the uncertainties in the actual modeling of hyperon matter [13–15].

Astrophysical data can also be employed to reduce the model uncertainties. For instance the presence of hyperons

in NSs may impact their cooling, by influencing neutrino emission processes. More precisely, two hyperon β decays, namely, $\Sigma^- \rightarrow \Lambda + e^- + \bar{\nu}$ and $\Lambda \rightarrow p + e^- + \bar{\nu}$, contributing to the direct URCA process, have been predicted to be very efficient in the long-time (\gg years) cooling of NSs [16]. If these processes occur, the surface temperature would be lower than the observed ones [17–19]. Therefore, it is necessary to reduce their efficiency, for instance, when the NS temperature is below the critical temperature T_C^Λ for Λ pairing [18,20–22]. If hyperons are present in NSs, the observed surface temperature is a sign for the existence of pairing among hyperons: in this superfluid state, the emissivity of strange decay reactions is reduced by a factor of $\exp(-\Delta/kT)$, where Δ represents the pairing gap [18].

In conclusion of these first remarks, the composition of dense matter in the core of NSs and PNSs has observational consequences which can be related to the properties of hyperon interactions. In addition, the impact of these interactions on the Λ -pairing gap is very important for the cooling of these stellar objects, and several theoretical predictions on Λ pairing have been performed in baryonic matter [23–31] and hypernuclei [32–43].

We briefly review these predictions. Based on a G -matrix, the Λ -pairing gap has been predicted to be about a few 100 keV [23] for densities $n_\Lambda \approx n_{\text{sat}}$, where n_{sat} is the saturation density of symmetric matter, $n_{\text{sat}} \approx 0.155 \pm 0.005 \text{ fm}^{-3}$ [24], and the BCS relation obtained in the weak-coupling approximation $k_B T_C \approx 0.57 \Delta^{T=0}$ has been found to be well satisfied [25–27]. Moreover, superfluidity has been predicted to occur at about $4n_{\text{sat}}$ in β -equilibrated matter, using one-boson-exchange potentials for the $\Lambda\Lambda$ interaction [28,29]. Phenomenological nuclear interactions have also been employed to predict the properties of Λ pairing in nuclear matter. For instance, a relativistic mean-field (RMF) model has predicted the pairing gap to be 810 keV at the baryon density of 0.349 fm^{-3} [30]. Other models consider σ^* and φ mesons (with strange quark) added on top of the other (without strange quark) mesons: the pairing gap is predicted to be reduced down to 282 keV at the total baryon density of 0.364 fm^{-3} [31]. These results illustrate the variability among different predictions.

One can also employ hypernuclei as a benchmark for $\Lambda\Lambda$ interactions. For instance, a study based on the relativistic Thomas-Fermi approach and applied to hypernuclei, has shown an interesting effect of the temperature: the Λ radii increase faster as a function of the temperature than the nucleon radii, since it is easier to excite the small amount of hyperons than to excite the large number of nucleons [32]. Still in finite nuclei, the Skyrme-Hartree-Fock model [33–35], the generalized liquid-drop model [36,37], and the beyond-mean-field SHF model [38–40] have been employed within the BCS approximation. Microscopic calculations applied to multi- Λ hypernuclei have emphasized the connection between pairing in the Λ channel and the $\Lambda\Lambda$ interaction [41–43]. Using different methods to calibrate the Λ -pairing strength, these studies have predicted the properties of multi- Λ hypernuclei in their ground states. However, there are no calculations in hypernuclei which explicitly treat temperature and Λ pairing together.

The main purpose of the present study is to understand the effect of temperature and Λ pairing in hypernuclei, in view of the future production of a wealth of hypernuclei at FAIR and JPARC. It is also expected to impact hyperon matter in astrophysics. In this work, we extend our previous analysis of Λ pairing in multistrange hypernuclei [41] by incorporating the finite-temperature effect. To do so, we implement the finite-temperature Hartree-Fock-Bogoliubov approach [44], where we consider Skyrme-type energy density functionals in the nucleon channel. To account for the ΛN interaction, we consider the density functionals DF-NSC89, DF-NSC97a, and DF-NSC97f, adjusted to reproduce Brueckner Hartree-Fock results based on Nijmegen interactions NSC89, NSC97a, and NSC97f [45,46]. To describe the $\Lambda\Lambda$ interaction, we use the empirical prescription EmpC [47], which is adjusted to reproduce the binding energy of ${}^6_{\Lambda\Lambda}\text{He}$.

In practice, we consider spherical symmetry in this first study, aiming at having a qualitative understanding of Λ pairing at finite temperature. We have, therefore, specifically chosen hypernuclei with closed proton and neutron shells, such as ${}^{40}_{-S\Lambda}\text{Ca}$, ${}^{132}_{-S\Lambda}\text{Sn}$, and ${}^{208}_{-S\Lambda}\text{Pb}$, known for their semimagic properties. Moreover, the structure of hyperon drip-line hypernuclei is also examined, particularly those with open neutron shells located near closed neutron shells, such as ${}^{56,58,62,64}_{20\Lambda}\text{Ca}$, ${}^{168,170,174,176}_{40\Lambda}\text{Sn}$, and ${}^{274,276,280,282}_{70\Lambda}\text{Pb}$. Our study focuses on investigating the impact of the temperature on the low-energy properties of multi- Λ hypernuclei.

The present manuscript is organized as follows. In Sec. II, we provide a brief overview of the FT-HFB approach applied to multi- Λ hypernuclei. In Sec. III, we explore the interplay between temperature and Λ pairing, analyzing their impact on the low-energy properties. Conclusions are given in Sec. IV.

II. FINITE-TEMPERATURE HARTREE-FOCK-BOGOLIUBOV APPROACH FOR MULTI- Λ HYPERNUCLEI

The present model is based on the FT-HFB approach, which is described in detail in Ref. [44]. It is a nonrelativistic model for nucleons $N = (p, n)$ and Λ hyperons, which is employed to describe multi- Λ hypernuclei.

A. Formalism

The total Hamiltonian reads

$$\hat{H} = \sum_i \hat{T}_i + \sum_{i,j} \hat{H}'_{ij}, \quad (1)$$

where \hat{T} represents the kinetic energy operators, and \hat{H}' denotes the interaction operator with $(i, j) = (N, N)$, (N, Λ) , and (Λ, Λ) . The total energy can be expressed as

$$E = \int d^3r \sum_{i,j} \epsilon_{ij}, \quad (2)$$

with the following contributions: the hyperon-nucleon energy density

$$\begin{aligned} \epsilon_{\Lambda N} = & -(\alpha_1 - \alpha_2 \rho_N + \alpha_3 \rho_N^2) \rho_\Lambda \rho_N \\ & + (\alpha_4 - \alpha_5 \rho_N + \alpha_6 \rho_N^2) \rho_\Lambda^{5/3} \rho_N, \end{aligned} \quad (3)$$

TABLE I. Parameters corresponding to the energy density and effective mass of the Λ hyperons.

Functional	α_1	α_2	α_3	α_4	α_5	α_6	α_7	α_8	α_9	μ_1	μ_2	μ_3	μ_4
DF-NSC89 + EmpC	327	1159	1163	335	1102	1660	22.81	0	0	1	1.83	5.33	6.07
DF-NSC97a + EmpC	423	1899	3795	577	4017	11061	21.12	0	0	0.98	1.72	3.18	0
DF-NSC97f + EmpC	384	1473	1933	635	1829	4100	33.25	0	0	0.93	2.19	3.89	0

the hyperon-hyperon energy density

$$\epsilon_{\Lambda\Lambda} = \frac{\hbar^2}{2m_\Lambda} \tau_\Lambda - (\alpha_7 - \alpha_8 \rho_\Lambda + \alpha_9 \rho_\Lambda^2) \rho_\Lambda^2, \quad (4)$$

and the nucleon-nucleon energy density, where q stands for neutrons or protons,

$$\begin{aligned} \epsilon_{\text{NN}} = & \frac{\hbar^2}{2m_{\text{N}}} \tau_{\text{N}} + \frac{1}{2} t_0 \left[\left(1 + \frac{x_0}{2}\right) \rho_{\text{N}}^2 - \left(x_0 + \frac{1}{2}\right) \sum_q \rho_q^2 \right] \\ & + \frac{t_1}{4} \left\{ \left(1 + \frac{x_1}{2}\right) \left[\rho_{\text{N}} \tau_{\text{N}} + \frac{3}{4} (\nabla \rho_{\text{N}})^2 \right] - \left(x_1 + \frac{1}{2}\right) \right. \\ & \times \sum_q \left[\rho_q \tau_q + \frac{3}{4} (\nabla \rho_q)^2 \right] \left. \right\} \\ & + \frac{t_2}{4} \left\{ \left(1 + \frac{x_2}{2}\right) \left[\rho_{\text{N}} \tau_{\text{N}} - \frac{1}{4} (\nabla \rho_{\text{N}})^2 \right] + \left(x_2 + \frac{1}{2}\right) \right. \\ & \times \sum_q \left[\rho_q \tau_q - \frac{1}{4} (\nabla \rho_q)^2 \right] \left. \right\} \\ & - \frac{1}{16} (t_1 x_1 + t_2 x_2) J_{\text{N}}^2 + \frac{1}{16} (t_1 - t_2) \sum_q J_q^2 \\ & + \frac{1}{12} t_3 \rho_{\text{N}}^\gamma \left[\left(1 + \frac{x_3}{2}\right) \rho_{\text{N}}^2 - \left(x_3 + \frac{1}{2}\right) \sum_q \rho_q^2 \right] \\ & + \frac{1}{2} W_0 \left(J_{\text{N}} \nabla \rho_{\text{N}} + \sum_q J_q \nabla \rho_q \right) + \epsilon_{\text{Coul}}. \quad (5) \end{aligned}$$

The parameters α_{1-9} in Eqs. (3) and (4) are provided in Table I for the following functionals: DF-NSC89, DF-NSC97a, and DF-NSC97f [45,46] with EmpC prescription for α_7 [47]. The density ρ_Λ represents the Λ density, and the nucleon density is $\rho_{\text{N}} = \rho_p + \rho_n$. In infinite nuclear matter, the kinetic energy densities τ_Λ and τ_{N} are analytical functions of the matter density: $\tau_i = \frac{3}{5} (6\pi^2/g_i)^{2/3} \rho_i^{5/3}$, where $g_i = 4(2)$ for $i = \text{N}(\Lambda)$. The parameters t_{0-3} , x_{0-3} , γ , and W_0 are given by the Skyrme interaction and J represents the spin-current densities of nucleons. The term ϵ_{Coul} corresponds to the Coulomb energy density. It is worth noting that, in Eqs. (3) and (4), we employ energy density functionals, which have been adjusted to reproduce Brueckner-Hartree-Fock predictions, incorporating both nucleons and Λ hyperons [45,46], as well as the bond energy of ${}^6_{\Lambda\Lambda}\text{He}$.

The HFB equations in coordinate representation are derived by taking the variation of the energy functional expressed in Eq. (2) with respect to the density matrices:

$$\begin{pmatrix} h - \lambda & \tilde{h} \\ \tilde{h} & -h + \lambda \end{pmatrix} \begin{pmatrix} U_k \\ V_k \end{pmatrix} = E_k \begin{pmatrix} U_k \\ V_k \end{pmatrix}, \quad (6)$$

where $h(\mathbf{r}\sigma, \mathbf{r}'\sigma') = \frac{\delta E}{\delta \rho(\mathbf{r}\sigma, \mathbf{r}'\sigma')}$ is the Hamiltonian containing the self-consistent field with particle density $\rho(r, r') = \frac{1}{4\pi} \sum_k (2j_k + 1) V_k(r) V_k^*(r')$ and the chemical potential λ , and $\tilde{h}(\mathbf{r}\sigma, \mathbf{r}'\sigma') = \frac{\delta E}{\delta \tilde{\rho}(\mathbf{r}\sigma, \mathbf{r}'\sigma')}$ is the pairing field with pairing density $\tilde{\rho}(r, r') = -\frac{1}{4\pi} \sum_k (2j_k + 1) V_k(r) U_k^*(r')$. The fields U_k and V_k are the components of the radial HFB wave function and E_k is the quasiparticle energy. It should be noted that the considered model incorporates two distinct types of HFB mean-field potentials:

$$V_\Lambda = \frac{\partial(\epsilon_{\Lambda\text{N}} + \epsilon_{\Lambda\Lambda})}{\partial \rho_\Lambda} - \left(\frac{m_\Lambda}{m_\Lambda^*(\rho_{\text{N}})} - 1 \right) \frac{(3\pi^2)^{2/3}}{2m_\Lambda} \rho_\Lambda^{2/3} \quad (7)$$

and

$$\begin{aligned} V_{\text{N}} = & \frac{\partial(\epsilon_{\Lambda\text{N}} + \epsilon_{\text{NN}})}{\partial \rho_{\text{N}}} + \frac{\partial}{\partial \rho_{\text{N}}} \left(\frac{m_\Lambda}{m_\Lambda^*(\rho_{\text{N}})} \right) \\ & \times \left(\frac{\tau_\Lambda}{2m_\Lambda} - \frac{3(3\pi^2)^{2/3}}{5} \frac{\rho_\Lambda^{5/3}}{2m_\Lambda} \right). \quad (8) \end{aligned}$$

The Λ effective mass reads

$$\frac{m_\Lambda^*(\rho_{\text{N}})}{m_\Lambda} = \mu_1 - \mu_2 \rho_{\text{N}} + \mu_3 \rho_{\text{N}}^2 - \mu_4 \rho_{\text{N}}^3, \quad (9)$$

where the parameters μ_{1-4} are given in Table I. The $\Lambda\Lambda$ -pairing interaction is defined as a volume-type contact interaction, similar to the one used in Ref. [41]:

$$V_{\Lambda\text{pair}} = V_{\Lambda_0} \delta(\mathbf{r}_1 - \mathbf{r}_2), \quad (10)$$

where V_{Λ_0} is the $\Lambda\Lambda$ -pairing-interaction strength. It should be noted that the pairing effect in the $\Lambda\Lambda$ channel is yet hypothetical. Nevertheless, even in the case of vanishing pairing, temperature effects shall impact the Λ -shell structure, through the Fermi distribution as described below.

All equations presented so far, including Eq. (6), are identical at finite temperature [44,48] provided the densities are generalized at finite temperature according to the following expressions:

$$\begin{aligned} \rho_T(r) = & \frac{1}{4\pi} \sum_k (2j_k + 1) \\ & \times [V_k^*(r) V_k(r) (1 - f_k) + U_k^*(r) U_k(r) f_k], \quad (11) \end{aligned}$$

$$\begin{aligned} \tau_T(r) = & \frac{1}{4\pi} \sum_k (2j_k + 1) \\ & \times \left\{ \left[\left(\frac{dV_k}{dr} - \frac{V_k}{r} \right)^2 + \frac{l_k(l_k + 1)}{r^2} V_k^2 \right] (1 - f_k) \right. \\ & \left. + \left[\left(\frac{dU_k}{dr} - \frac{U_k}{r} \right)^2 + \frac{l_k(l_k + 1)}{r^2} U_k^2 \right] f_k \right\}, \quad (12) \end{aligned}$$

TABLE II. $\Lambda\Lambda$ -pairing-interaction strength and corresponding hyperisotopic chain for each functional.

Functional	V_{Λ_0} (MeV fm ³)	Hyperisotopic chain
DF-NSC89 + EmpC	-139	${}^{40-S}_{-S\Lambda}\text{Ca}$ ($-S = 6-20$)
DF-NSC97a + EmpC	-148	${}^{40-S}_{-S\Lambda}\text{Ca}$ ($-S = 6-20$)
DF-NSC97f + EmpC	-180	${}^{40-S}_{-S\Lambda}\text{Ca}$ ($-S = 6-20$)
DF-NSC89 + EmpC	-158	${}^{132-S}_{-S\Lambda}\text{Sn}$ ($-S = 18-40$)
DF-NSC97a + EmpC	-145	${}^{132-S}_{-S\Lambda}\text{Sn}$ ($-S = 18-40$)
DF-NSC97f + EmpC	-180	${}^{132-S}_{-S\Lambda}\text{Sn}$ ($-S = 18-40$)
DF-NSC89 + EmpC	-184	${}^{208-S}_{-S\Lambda}\text{Pb}$ ($-S = 58-70$)
DF-NSC97a + EmpC	-180	${}^{208-S}_{-S\Lambda}\text{Pb}$ ($-S = 58-70$)
DF-NSC97f + EmpC	-220	${}^{208-S}_{-S\Lambda}\text{Pb}$ ($-S = 58-70$)

$$J_T(r) = \frac{1}{4\pi} \sum_k (2j_k + 1) \left[j_k(j_k + 1) - l_k(l_k + 1) - \frac{3}{4} \right] \times \{V_k^2(1 - f_k) + U_k^2 f_k\}, \quad (13)$$

where $f_k = [1 + \exp(E_k/k_B T)]^{-1}$ is the Fermi distribution, k_B is the Boltzmann constant, and T is the temperature. The low-energy properties in the equilibrium state at finite temperature for multi- Λ hypernuclei are obtained from the solution of Eq. (6), injecting Eqs. (11)–(13) into Eqs. (2)–(9).

B. Numerical strategy

The FT-HFB equations for the multi- Λ hypernuclei presented above are solved in coordinate representation and considering spherical symmetry. The SLy5 Skyrme interaction is fixed for the nucleon sector since it accurately reproduces stable and exotic nuclei properties [49]. As usual, the spin-orbit term in the Λ mean-field channel is neglected (see Ref. [50], for instance).

Following the approach suggested in Ref. [41], the strength of the $\Lambda\Lambda$ -pairing interaction V_{Λ_0} is adjusted to reproduce the maximum value of the theoretical BCS prediction in uniform matter calculated in Ref. [28] (see Table II). It should be noted that the pairing gap at $T = 0$ in nuclei is expected to be close to the one of uniform matter. For instance, in the considered $-S$ intervals displayed in Table II, the average pairing gap $\bar{\Delta}_\Lambda(T = 0)$ (running over a set of hypernuclei changing the number of hyperons while keeping the number of protons and neutrons) is close to the value in uniform matter [41]. It should be noted that calculations of the average pairing gaps at finite temperatures are carried out using equation

$$\bar{\Delta}_\Lambda(T) \equiv \frac{1}{N_S} \sum_{-S} \Delta_\Lambda(T, {}^{A-S}_{-S\Lambda}X), \quad (14)$$

where N_S represents the count of hyperisotopes within the observed range.

We employ the Numerov method to solve the FT-HFB equations and we consider the Dirichlet boundary condition for vanishing wave functions. The wave functions are obtained

numerically for a spherical box with a radius of 30 fm and a resolution of 0.1 fm. The self-consistent solution is obtained by an iterative process, which is repeated until the total energy converges within an accuracy of about 10^{-8} MeV.

III. RESULTS AT FINITE TEMPERATURES

In this section, we investigate how the pairing gaps, condensation energies, normal and pairing densities, and radii of multi- Λ hypernuclei evolve as functions of the temperature, considering different numbers of Λ hyperons ($-S$) present in the system. We focus on studying the hyperisotopes ${}^{40-S}_{-S\Lambda}\text{Ca}$, ${}^{132-S}_{-S\Lambda}\text{Sn}$, and ${}^{208-S}_{-S\Lambda}\text{Pb}$ being magic in the nucleon sector. Additionally, in cases where the hypernuclei are close to the hyperon drip-line, investigations have also explored hypernuclei with neutron open-shell configurations at neutron numbers lying between ± 2 and ± 4 from the neutron magic number.

A. Λ -pairing gaps and binding energies

We first study the Λ -pairing gap (Δ_Λ) as a function of the temperature in the following multi- Λ hyperisotopes: ${}^{40-S}_{-S\Lambda}\text{Ca}$, ${}^{132-S}_{-S\Lambda}\text{Sn}$, and ${}^{208-S}_{-S\Lambda}\text{Pb}$. The results for $\Delta_\Lambda(T)$ are shown in Fig. 1, using the DF-NSC97a + EmpC functional.

As the temperature increases, the pairing gaps Δ_Λ decrease until temperature reaches the critical temperature T_C^Λ for Λ pairing, which is studied in more detail in the following. At low temperature, the pairing gap is only weakly reduced but it drops down only when the temperature is close to the critical temperature T_C^Λ . Note that for hypernuclei with $-S$ close to magic numbers, the pairing gap drops to zero even before the critical temperature is reached, at about $k_B T = 0.4$ MeV. This trend is visible in Fig. 2, illustrating the influence of strangeness on finite temperature across various functionals for ${}^{40-S}_{-S\Lambda}\text{Ca}$ hypernuclei. In the three panels of Fig. 1, the largest temperature is set to the maximal critical temperature T_C^Λ for the considered hyperisotopic chain (e.g., 0.54 MeV in the ${}^{40-S}_{-S\Lambda}\text{Ca}$ case).

In ${}^{40-S}_{-S\Lambda}\text{Ca}$, the Λ -pairing gap Δ_Λ is maximum at $-S = 6$ in the studied range $-S = 6-20$. Similarly, for ${}^{132-S}_{-S\Lambda}\text{Sn}$, the maximum pairing gap is obtained at $-S = 28$ in the range $-S = 18-40$, and for ${}^{208-S}_{-S\Lambda}\text{Pb}$, it occurs at $-S = 64$ in the range $-S = 58-70$. The pairing gaps are quenched for the following magic numbers: $-S = 8, 18, 20, 34, 40, 58, \text{ and } 70$. This sequence is different from the usual one in nonstrange nuclei since the spin-orbit has a negligible impact in the Λ channel, involving a different shell structure.

It should be noted that qualitatively similar results are obtained for the DF-NSC89 + EmpC and DF-NSC97f + EmpC functionals. This can be seen in Fig. 3 for ${}^{46}_{6\Lambda}\text{Ca}$, ${}^{160}_{28\Lambda}\text{Sn}$, and ${}^{272}_{64\Lambda}\text{Pb}$ hypernuclei. Comparing Δ_Λ values for all three functionals, the DF-NSC97a + EmpC functional exhibits the largest Λ -pairing-gap value across almost all temperatures. While a larger density of states around the Fermi level generally contributes to the enhanced pairing gap, for the hypernuclei we are looking at, the increased number of bound single-particle states expands the available states for pairing interactions. This leads to a larger pairing gap, driven by the

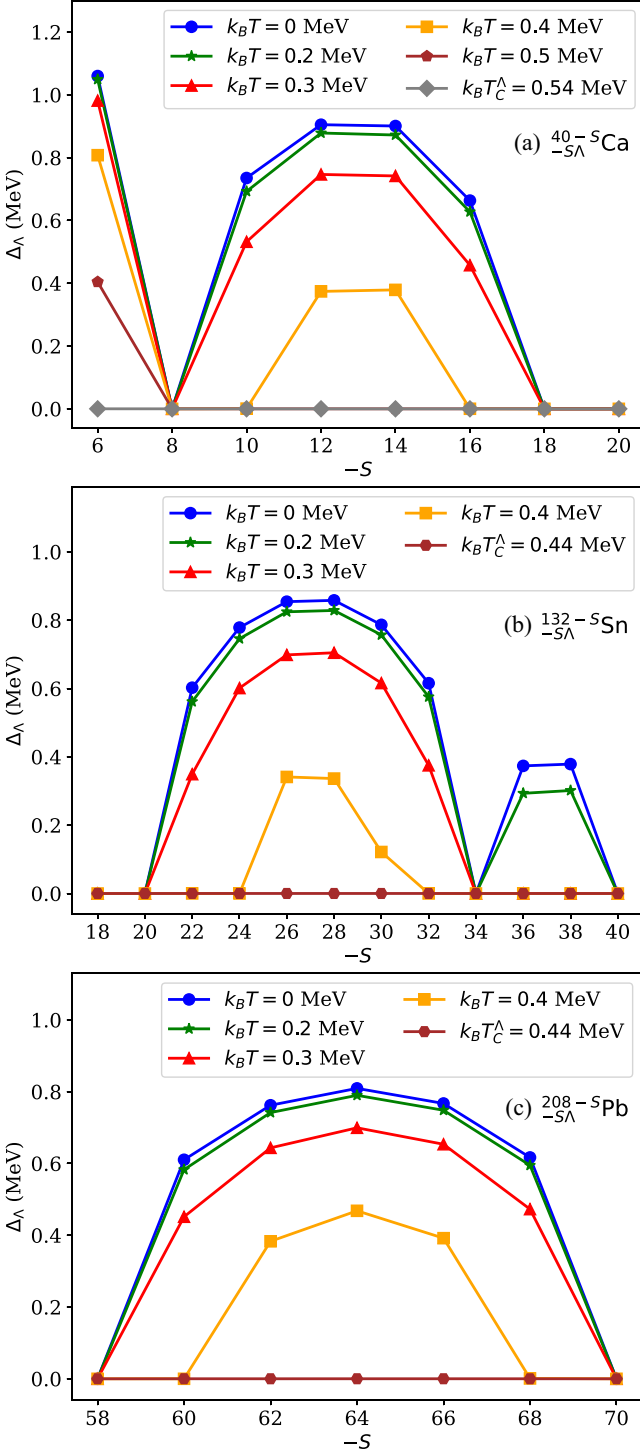


FIG. 1. Evolution of the Λ -pairing gap with increasing temperature for ${}^{40}_{-\Lambda}\text{Ca}$ (a), ${}^{132}_{-\Lambda}\text{Sn}$ (b), and ${}^{208}_{-\Lambda}\text{Pb}$ (c) hypernuclei using the DF-NSC97a + EmpC functional.

deeper $N\Lambda$ potential of the DF-NSC97a + EmpC functional compared to DF-NSC89 + EmpC and DF-NSC97f + EmpC [10,11].

Table III displays the values of the pairing gaps in the ground state $\Delta_{\Lambda}^{T=0}$ and the critical temperature T_C^{Λ} for a set of hypernuclei. We find that the BCS relation in uniform

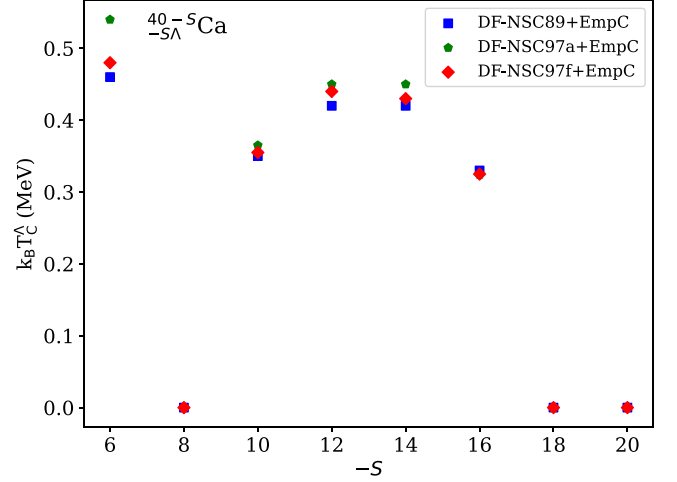


FIG. 2. Impact of strangeness on finite temperature for ${}^{40}_{-\Lambda}\text{Ca}$ hypernuclei.

matter, namely, $k_B T_C \approx 0.5 \Delta_{\Lambda}^{T=0}$, is well reproduced for finite hypernuclei. Note that the BCS relation is almost independent of the functional, since all used functionals impact both $\Delta_{\Lambda}^{T=0}$ and T_C^{Λ} .

The effects of finite temperatures and pairing correlations on binding energy can also be assessed by estimating the condensation energy, defined as $E_{\text{cond}} = E_{\text{HF}} - E_{\text{HFB}}$. Figure 4 shows E_{cond} for a set of ${}^{132}_{-\Lambda}\text{Sn}$ hypernuclei, using DF-NSC89 + EmpC, DF-NSC97a + EmpC, and DF-NSC97f + EmpC functionals. The behavior of the condensation energy closely mirrors the trend observed in the Λ -pairing gap of Fig. 1.

The peak value of the condensation energy nearly reaches 3 MeV at $T = 0$. With increasing temperature, the $E_{\text{HF}} - E_{\text{HFB}}$ value experiences a consistent reduction across all hypernuclei, mirroring the pattern displayed in Fig. 1. For instance, as the temperature increases to $k_B T = 0.3$ MeV, the peak of the condensation energy decreases to approximately 2 MeV. At a specific temperature threshold $E_{\text{HF}} = E_{\text{HFB}}$ across the whole $-S$ range. In conclusion, Fig. 4 represents the

TABLE III. Pairing gap in the ground state $\Delta_{\Lambda}^{T=0}$ and critical temperatures T_C^{Λ} for different functionals and for a set of hypernuclei, which are the ones with maximum pairing gap (see Fig. 1).

Functional	Hypernucleus	$\Delta_{\Lambda}^{T=0}$ (MeV)	$k_B T_C^{\Lambda}$ (MeV)
DF-NSC89 + EmpC	${}^{46}_{6\Lambda}\text{Ca}$	0.82	0.46
DF-NSC97a + EmpC	${}^{46}_{6\Lambda}\text{Ca}$	1.04	0.54
DF-NSC97f + EmpC	${}^{46}_{6\Lambda}\text{Ca}$	0.98	0.48
DF-NSC89 + EmpC	${}^{160}_{28\Lambda}\text{Sn}$	0.84	0.43
DF-NSC97a + EmpC	${}^{160}_{28\Lambda}\text{Sn}$	0.82	0.44
DF-NSC97f + EmpC	${}^{160}_{28\Lambda}\text{Sn}$	0.82	0.43
DF-NSC89 + EmpC	${}^{272}_{64\Lambda}\text{Pb}$	0.69	0.39
DF-NSC97a + EmpC	${}^{272}_{64\Lambda}\text{Pb}$	0.76	0.44
DF-NSC97f + EmpC	${}^{272}_{64\Lambda}\text{Pb}$	0.71	0.38

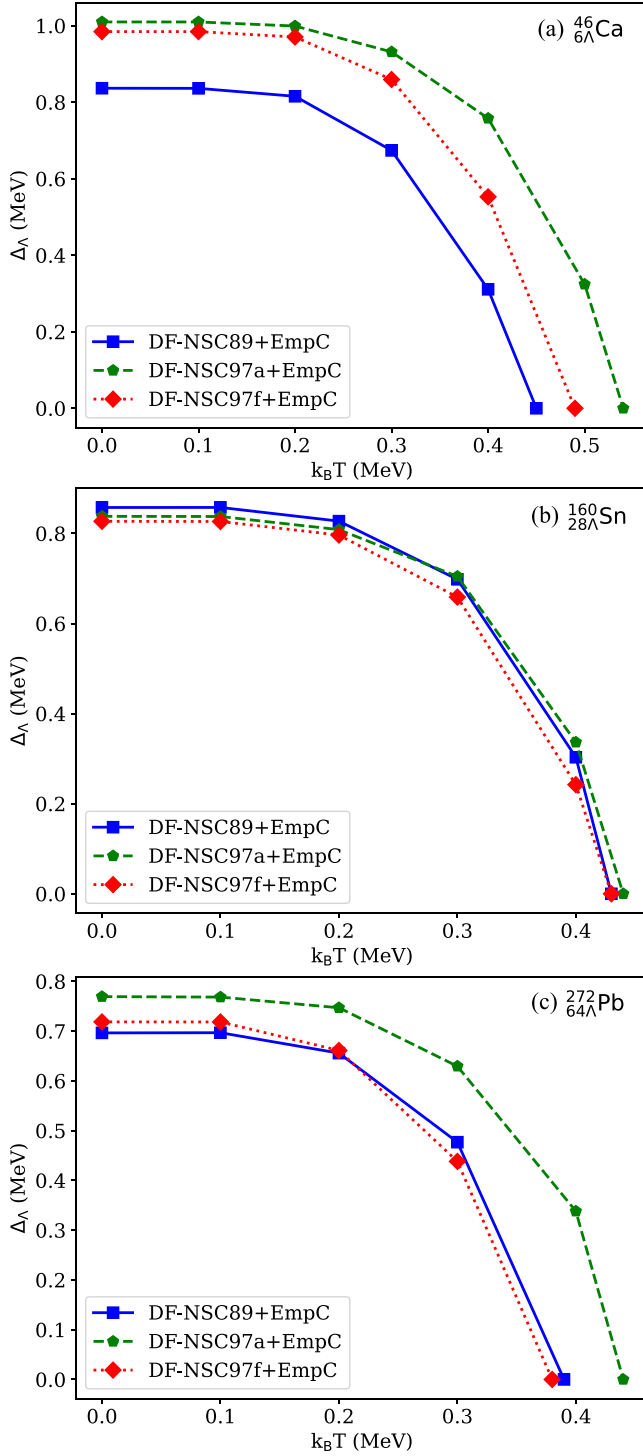


FIG. 3. Evolution of Λ -pairing gap with increasing temperature for $^{46}_{6\Lambda}\text{Ca}$ (a), $^{160}_{28\Lambda}\text{Sn}$ (b), and $^{272}_{64\Lambda}\text{Pb}$ (c) hypernuclei. The plot depicts the results obtained from three functionals: DF-NSC89 + EmpC (solid line), DF-NSC97a + EmpC (dashed line), and DF-NSC97f + EmpC (dotted line).

condensation energy for various temperatures up to the critical one ($T_c = 0.44$ MeV). It shows a systematic decrease as the temperature increases, and at the critical temperature, the FT-HF results are recovered. Figure 5 shows this for the

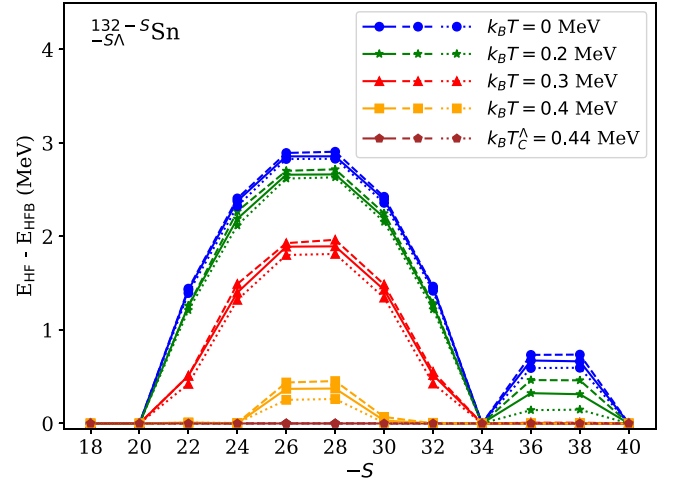


FIG. 4. Temperature-dependent binding energy differences of HF and HFB approaches for $^{132-S}_{-S\Lambda}\text{Sn}$ hypernuclei with different functionals. The plot depicts the results obtained from three functionals: DF-NSC89 + EmpC (solid line), DF-NSC97a + EmpC (dashed line), and DF-NSC97f + EmpC (dotted line).

average pairing gap defined by Eq. (14) in the case of the DF-NSC89 + EmpC and DF-NSC97f + EmpC functionals. This figure also shows that the definition of the average pairing gap defined in Eq. (14) still allows behavior as a function of A similar to the nucleonic one, i.e., $\bar{\Delta}_\Lambda \sim c/\sqrt{A}$. The A slope is slightly larger as the temperature increases.

B. Normal and abnormal pairing densities

Figure 6 displays the density profiles for three typical hypernuclei, $^{46}_{6\Lambda}\text{Ca}$, $^{160}_{28\Lambda}\text{Sn}$, and $^{272}_{64\Lambda}\text{Pb}$, for $T = 0$ and $T = T_c^\Lambda$. The impact of temperature on the normal densities is very small in the range of temperature bounded by the critical

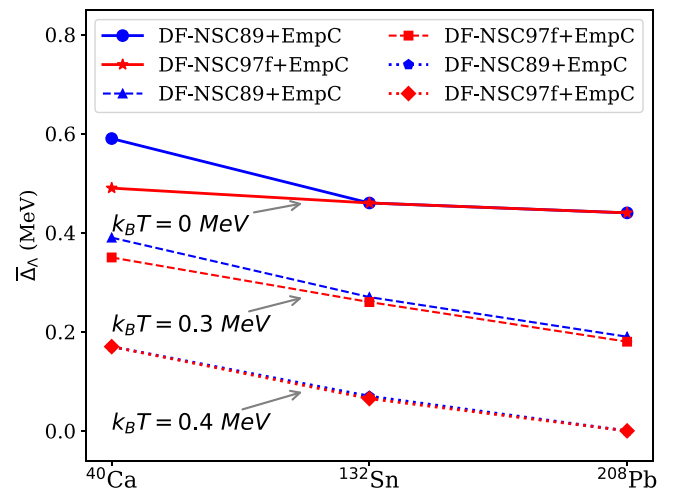


FIG. 5. Variations in average pairing gap computed using Eq. (14) for $^{40-S}_{-S\Lambda}\text{Ca}$ ($-S = 6-20$), $^{132-S}_{-S\Lambda}\text{Sn}$ ($-S = 18-40$), and $^{208-S}_{-S\Lambda}\text{Pb}$ ($-S = 58-70$) hypernuclei. The plot depicts the results obtained from three temperatures: $k_B T = 0$ MeV (solid lines), $k_B T = 0.3$ MeV (dashed lines), and $k_B T = 0.4$ MeV (dotted lines).

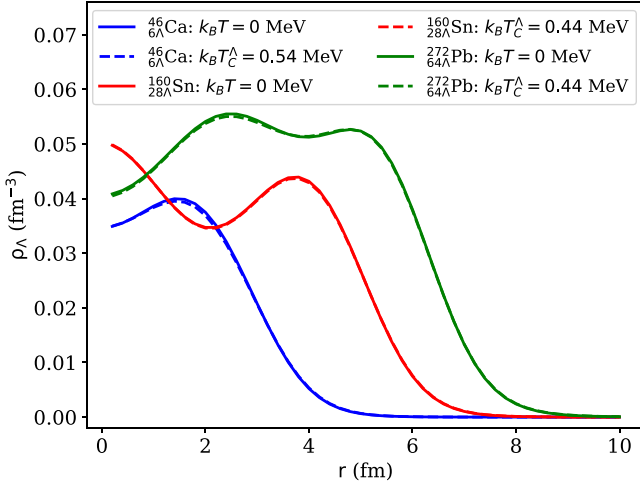


FIG. 6. Normal density profiles of $^{46}_{6\Lambda}\text{Ca}$, $^{160}_{28\Lambda}\text{Sn}$, and $^{272}_{64\Lambda}\text{Pb}$ hypernuclei at finite temperatures using the DF-NSC97a + EmpC functional.

temperature. The Λ single-particle spectrum has also been analyzed. In the considered hypernuclei, shifts in energy levels of up to a few hundred keV are observed, as temperature increases. Therefore, there is not an important impact of the temperature of the Λ single-particle spectrum.

The Λ -hyperon radius, along with the nuclear radius, is also analyzed. It should be noted that the value calculated here using only neutron and proton densities is referred to as the nuclear radius. Figure 7 illustrates this in the hypernuclei $^{46}_{6\Lambda}\text{Ca}$, $^{160}_{28\Lambda}\text{Sn}$, and $^{272}_{64\Lambda}\text{Pb}$ using the DF-NSC97a + EmpC functional. Small effects of temperature are found. Across all examined hypernuclei, the modification in the Λ hyperon radii remains around 0.3% as temperature changes from 0 to T_C^Λ . Similarly, this change remains relatively small as the temperature extends from 0 to $2T_C^\Lambda$ for these

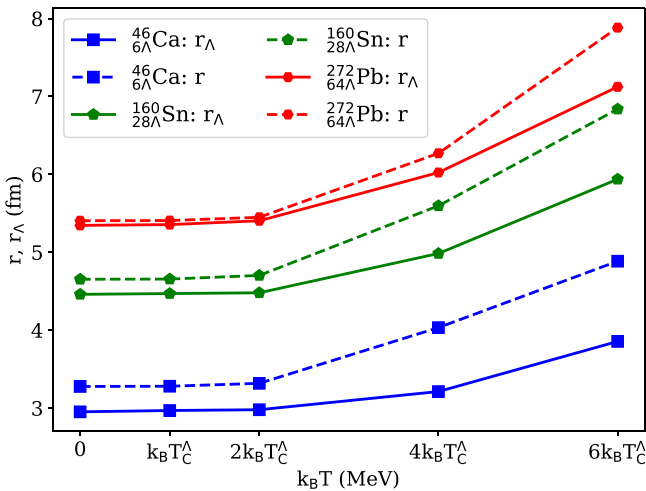


FIG. 7. Correlation between temperature and Λ -hyperon (solid lines) and nuclear (dashed lines) radii in hypernuclei $^{46}_{6\Lambda}\text{Ca}$, $^{160}_{28\Lambda}\text{Sn}$, and $^{272}_{64\Lambda}\text{Pb}$ using the DF-NSC97a + EmpC functional. Corresponding $k_B T_C^\Lambda$ values of these hypernuclei are listed in Table III.

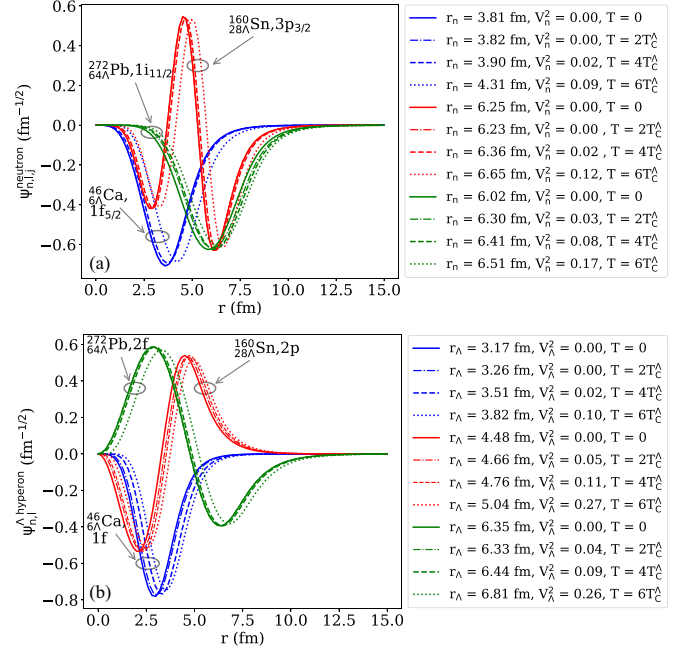


FIG. 8. Temperature dependence of neutron (a) and Λ -hyperon (b) canonical wave functions for $^{46}_{6\Lambda}\text{Ca}$, $^{160}_{28\Lambda}\text{Sn}$, and $^{272}_{64\Lambda}\text{Pb}$ hypernuclei, which contribute the most to the increase in radii shown in Fig 7. The label segments of panels (a) and (b) display the root-mean-square radii (r) and occupation probabilities (V^2) derived from the relevant states at varying temperatures.

hypernuclei. For instance, in the case of $^{40}_{-S}\text{Ca}$ hyperisotopes, the radius increase is roughly 0.6%, while for $^{132}_{-S}\text{Sn}$ hyperisotopes it reaches around 3%. In the scenario of Λ hyperon-rich $^{208}_{-S}\text{Pb}$, this increase amounts to approximately 4%. Figure 7 shows that the variation of nuclear radii with temperature closely mirrors the one of Λ -hyperon radii. The difference between nuclear radii and Λ -hyperon radii ($r - r_\Lambda$) remains relatively stable up to $2T_C^\Lambda$. Beyond this temperature, this difference increases, with a smaller effect on heavy hypernuclei. In conclusion, we found only weak impact of temperature on the Λ hyperon and nuclear radii. Beyond $2T_C$, the sudden increase of the radii is due to the creation of a neutron gas, which is a spurious effect of using a finite-size box [32].

In order to study more quantitatively the origin of the increase of the radii with temperature, we examined the wave functions of the states contributing to radius increases at temperatures exceeding $2T_C$, and we included the most significant ones in Fig. 8, in the canonical basis. The computed root-mean-square (rms) radii values for these states are shown in the inset, along with their occupation probabilities. Each of these states resides above the Fermi level, and at $T = 0$, their occupation probabilities are zero. As seen in Fig. 8, only at temperatures greater than $2T_C$ do the occupation probabilities of these states become large. Concurrently, the rms radii increase, and the wave functions are shifted to larger positions.

While the impact of temperature on normal density profiles has been found to be negligible, the effect of temperature

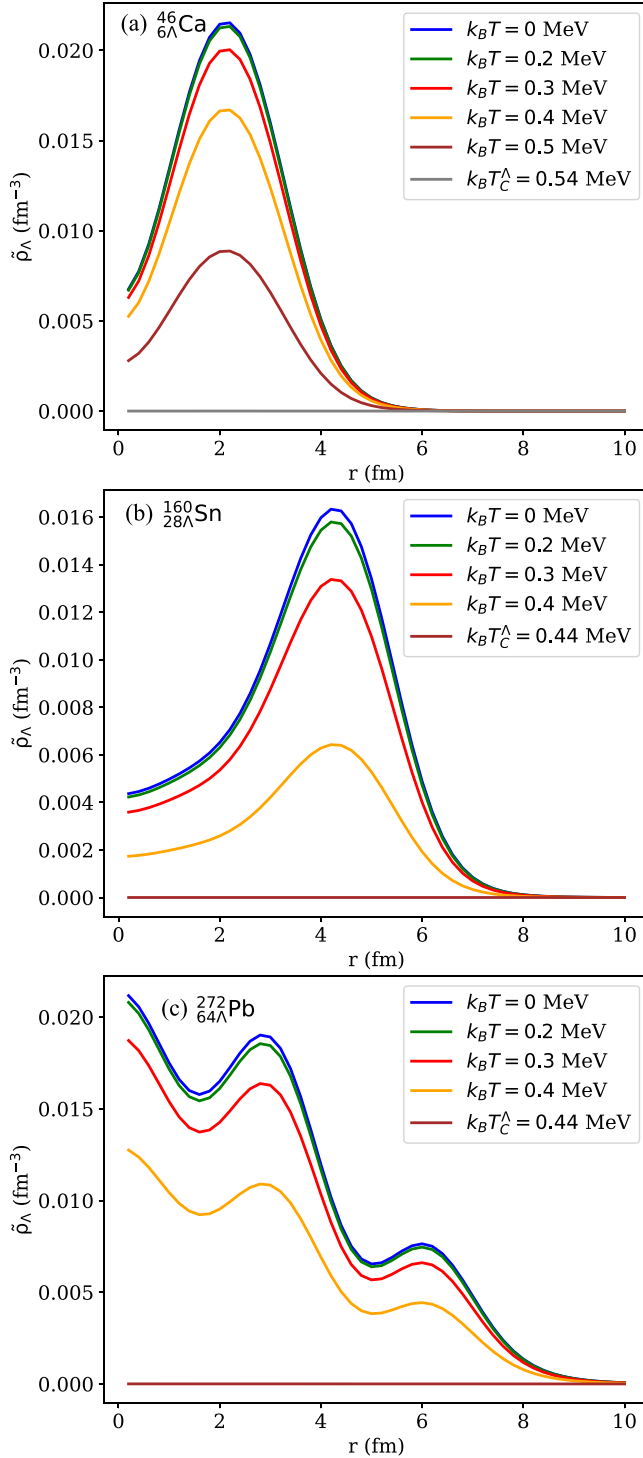


FIG. 9. Abnormal pairing density profiles for $^{46}_{64\Lambda}\text{Ca}$ (a), $^{160}_{28\Lambda}\text{Sn}$ (b), and $^{272}_{64\Lambda}\text{Pb}$ (c) hypernuclei at finite temperatures using the DF-NSC97a + EmpC functional.

on the abnormal pairing density profiles is much stronger, as shown in Fig. 9 for $^{46}_{64\Lambda}\text{Ca}$, $^{160}_{28\Lambda}\text{Sn}$, and $^{272}_{64\Lambda}\text{Pb}$ hypernuclei. Note that all the other hypernuclei that we have studied (see Fig. 1) show similar results. As expected, the reduction of the abnormal pairing density scales with the one of the pairing gaps shown in Fig. 1.

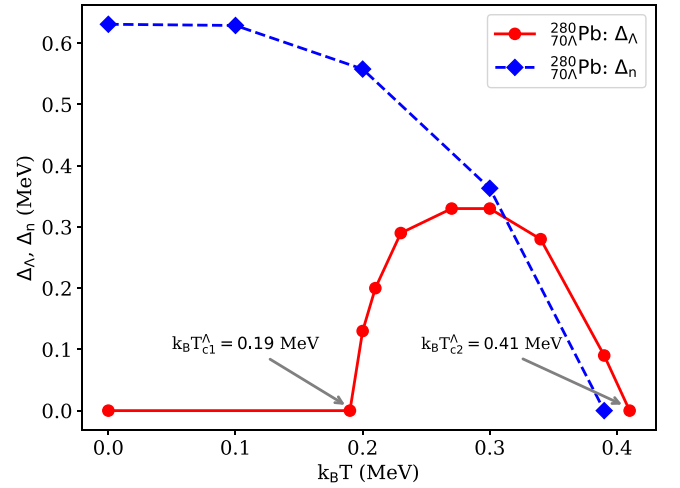


FIG. 10. Comparison of the evolution of Λ - and neutron-pairing gaps with increasing temperature for the $^{280}_{70\Lambda}\text{Pb}$ hypernucleus. The red line represents the Λ -pairing gap calculated using the DF-NSC97f + EmpC functional, while the blue line represents the neutron-pairing gap using a pairing strength of $V_{n0} = -265 \text{ MeV fm}^3$.

C. Pairing correlations around the hyperon drip-line

Among the $^{40-S}_{-S\Lambda}\text{Ca}$, $^{132-S}_{-S\Lambda}\text{Sn}$, and $^{208-S}_{-S\Lambda}\text{Pb}$ hypernuclei that we examined in detail above, $^{60}_{20\Lambda}\text{Ca}$, $^{172}_{40\Lambda}\text{Sn}$, and $^{278}_{70\Lambda}\text{Pb}$ lie the closest to the hyperon drip-line at $T = 0$: their Λ -separation energies are very close to 0. These drip-line systems can contribute to conditions where the pairing re-entrance effect (the pairing gap becomes nonzero above a given temperature) is predicted [51,52]. However, as seen from Fig. 1, even at finite temperatures, $\Delta_\Lambda = 0$ for these hypernuclei. This is not the case when considering open-shell neutron cases. For this purpose, calculations were performed for $^{56,58,62,64}_{20\Lambda}\text{Ca}$, $^{168,170,174,176}_{40\Lambda}\text{Sn}$, and $^{274,276,280,282}_{70\Lambda}\text{Pb}$ hypernuclei using all three functionals. Mixed-type pairing interaction was used in the neutron channel for these hypernuclei, with the pairing strength $V_{n0} = -265 \text{ MeV fm}^3$, such that the pairing gap $\Delta_n \approx 0.6 \text{ MeV}$ in $^{280}_{70\Lambda}\text{Pb}$ (see Fig. 10). For the Λ channel, we used the pairing strengths given in Table II. Pairing re-entrance occurs in $^{280}_{70\Lambda}\text{Pb}$ using the DF-NSC97f + EmpC functional, with the two predicted critical temperatures $k_B T_{c1} = 0.19 \text{ MeV}$ and $k_B T_{c2} = 0.41 \text{ MeV}$. It should be noted that at $k_B T_{c2} = 0.41 \text{ MeV}$, using the DF-NSC97f + EmpC functional yields chemical potentials of -0.32 MeV for Λ hyperons, -2.83 MeV for neutrons, and -7.21 MeV for protons in $^{280}_{70\Lambda}\text{Pb}$. However, for all other neutron open-shell hypernuclei we investigated, Δ_Λ remains constant at 0 across all temperatures. The reason for the pairing re-entrance phenomenon specific to $^{280}_{70\Lambda}\text{Pb}$ is that, in this hypernucleus using DF-NSC97f + EmpC, the energy difference between the last occupied $3s$ level and the first unoccupied $1h$ level is smaller compared to other similar $^{274,276,278,282}_{70\Lambda}\text{Pb}$ hypernuclei, as shown in Table IV. As the temperature changes, the $1h$ level, which is for this hypernucleus is empty at $T = 0$, begins to fill, and pairing properties begin to emerge at temperatures greater than $k_B T = 0.19 \text{ MeV}$.

TABLE IV. Energy difference between the highest occupied $3s$ level and the lowest unoccupied $1h$ level in $^{274,276,278,280,282}_{70\Lambda}\text{Pb}$ hypernuclei at $T = 0$.

Functionals	Energy difference (MeV)				
	$^{274}_{70\Lambda}\text{Pb}$	$^{276}_{70\Lambda}\text{Pb}$	$^{278}_{70\Lambda}\text{Pb}$	$^{280}_{70\Lambda}\text{Pb}$	$^{282}_{70\Lambda}\text{Pb}$
DF-NSC89 + EmpC	1.87	1.79	1.81	1.80	1.76
DF-NSC97a + EmpC	3.21	2.87	3.03	3.56	3.41
DF-NSC97f + EmpC	1.68	1.68	1.59	1.53	1.62

IV. CONCLUSIONS

In conclusion, the interplay between pairing and finite temperature for multi- Λ hypernuclei has been studied using the FT-HFB approach. We have considered three different functionals for the $N\Lambda$ channel, DF-NSC89, DF-NSC97a, and DF-NSC97f, all adjusted from microscopic Brueckner-Hartree-Fock predictions. For the $\Lambda\Lambda$ channel, the empirical prescription EmpC has been used, which is adjusted to reproduce the experimental bond energy in $^6_{\Lambda\Lambda}\text{He}$.

The pairing gaps for individual hypernuclei show similar trends as the temperature approaches the critical temperature T_C^Λ , which is found to be about 0.54 MeV and to scale with respect to $\Delta_\Lambda(T = 0)$ as suggested by the BCS relation. Among the studied functionals, DF-NSC97a + EmpC predicts the largest pairing gaps. While this difference is generally not

greater than 0.1–0.2 MeV, the DF-NSC97a + EmpC functional provides results similar to those of the DF-NSC89 + EmpC and DF-NSC97f + EmpC functionals for all investigated ground-state properties.

We have also investigated the effect of temperature on the binding energy, on the single-particle spectra, on the normal density, and on the Λ -hyperon radius. There is no effect of temperature for $T \lesssim T_C^\Lambda$. As expected, the abnormal pairing densities and the condensation energy are impacted by the temperature and shrink to zero for $T = T_C^\Lambda$. Calculations also explored hyperon drip-line hypernuclei. A pairing re-entrance effect was observed in the neutron open-shell hyperon drip-line hypernucleus $^{280}_{70\Lambda}\text{Pb}$, in the Λ channel.

In summary, this study clarifies the combined effects of temperature and pairing correlations in hypernuclei. Our main finding is that the usual BCS correlation between T_C^Λ and $\Delta_\Lambda(T = 0)$ remains valid for hypernuclei.

ACKNOWLEDGMENTS

This work is supported by the Scientific and Technological Research Council of Turkey (TÜBİTAK) under Project No. MFAG-118F098 and the Yıldız Technical University under Projects No. FBI-2018-3325 and No. FBA-2021-4229. This work is also supported by the LABEX Lyon Institute of Origins (Grant No. ANR-10-LABX-0066) of the *Université de Lyon* and the IN2P3 masterproject MAC.

- [1] A. Ravlic, E. Yuksel, T. Niksis, and N. Paar, Expanding the limits of nuclear stability at finite temperature, *Nat. Commun.* **14**, 4834 (2023).
- [2] S. Reddy, M. Prakash, J. M. Lattimer, and J. A. Pons, Effects of strong and electromagnetic correlations on neutrino interactions in dense matter, *Phys. Rev. C* **59**, 2888 (1999).
- [3] L. F. Roberts, G. Shen, V. Cirigliano, J. A. Pons, S. Reddy, and S. E. Woosley, Protoneutron star cooling with convection: The effect of the symmetry energy, *Phys. Rev. Lett.* **108**, 061103 (2012).
- [4] A. Burrows, Colloquium: Perspectives on core-collapse supernova theory, *Rev. Mod. Phys.* **85**, 245 (2013).
- [5] T. Foglizzo *et al.*, The explosion mechanism of core-collapse supernovae: Progress in supernova theory and experiments, *Publ. Astron. Soc. Aust.* **32**, e009 (2015).
- [6] U. R. Geppert, Thermal evolution of neutron stars, in *Handbook of Supernovae*, edited by A. W. Alsabti and P. Murdin (Springer, Cham, 2016), pp. 1–23.
- [7] W. Keil and H. T. Janka, Hadronic phase transitions at supranuclear densities and the delayed collapse of newly formed neutron stars, *Astron. Astrophys.* **296**, 145 (1995).
- [8] Z. Yu, G.-Z. Liu, M.-F. Zhu, Y. Xu, and E.-G. Zhao, Thermal neutron stars including the hyperon-hyperon interactions, *Nucl. Phys. A* **834**, 97c (2010).
- [9] J. Schaffner-Bielich, Strangeness in compact stars, *Nucl. Phys. A* **835**, 279 (2010).
- [10] E. K.-P. Collaboration, Double- Λ hypernuclei observed in a hybrid emulsion experiment, *Phys. Rev. C* **88**, 014003 (2013).
- [11] E. Khan, J. Margueron, F. Gulminelli, and A. R. Raduta, Microscopic evaluation of the hypernuclear chart with Λ hyperons, *Phys. Rev. C* **92**, 044313 (2015).
- [12] H. Ekawa, K. Agari, J. K. Ahn, T. Akaishi, Y. Akazawa, S. Ashikaga, B. Bassalleck, S. Bleser, Y. Endo, Y. Fujikawa, N. Fujioka, M. Fujita, R. Goto, Y. Han, S. Hasegawa, T. Hashimoto, S. H. Hayakawa, T. Hayakawa, E. Hayata, K. Hicks *et al.*, Observation of a Be double-Lambda hypernucleus in the J-PARC E07 experiment, *Prog. Theor. Exp. Phys.* **2019**, 021D02 (2019).
- [13] A. Feliciello and T. Nagae, Experimental review of hypernuclear physics: Recent achievements and future perspectives, *Rep. Prog. Phys.* **78**, 096301 (2015).
- [14] A. Gal, E. V. Hungerford, and D. J. Millener, Strangeness in nuclear physics, *Rev. Mod. Phys.* **88**, 035004 (2016).
- [15] H. Ohnishi, F. Sakuma, and T. Takahashi, Hadron physics at J-PARC, *Prog. Part. Nucl. Phys.* **113**, 103773 (2020).
- [16] F. Anzuini, A. Melatos, C. Dehman, D. Viganò, and J. A. Pons, Fast cooling and internal heating in hyperon stars, *Mon. Not. R. Astron. Soc.* **509**, 2609 (2021).
- [17] C. Schaab, F. Weber, M. K. Weigel, and N. K. Glendenning, Thermal evolution of compact stars, *Nucl. Phys. A* **605**, 531 (1996).
- [18] S. Tsuruta, Thermal properties and detectability of neutron stars. II. Thermal evolution of rotation-powered neutron stars, *Phys. Rep.* **292**, 1 (1998).
- [19] A. Y. Potekhin, D. A. Zyuzin, D. G. Yakovlev, M. V. Beznogov, and Y. A. Shibano, Thermal luminosities of cooling neutron stars, *Mon. Not. R. Astron. Soc.* **496**, 5052 (2020).

- [20] C. J. Pethick, Cooling of neutron stars, *Rev. Mod. Phys.* **64**, 1133 (1992).
- [21] D. Yakovlev, A. Kaminker, O. Gnedin, and P. Haensel, Neutrino emission from neutron stars, *Phys. Rep.* **354**, 1 (2001).
- [22] C. Schaab, S. Balberg, and J. Schaffner-Bielich, Implications of hyperon pairing for cooling of neutron stars, *Astrophys. J.* **504**, L99 (1998).
- [23] S. Balberg and N. Barnea, S -wave pairing of Λ hyperons in dense matter, *Phys. Rev. C* **57**, 409 (1998).
- [24] J. Margueron, R. Hoffmann Casali, and F. Gulminelli, Equation of state for dense nucleonic matter from metamodeling. I. foundational aspects, *Phys. Rev. C* **97**, 025805 (2018).
- [25] E. M. Lifshitz and L. P. Pitaevskii, *Statistical Physics* (Pergamon, Oxford, 1980), Vol. 2, pp. 152–158.
- [26] T. Takatsuka and R. Tamagaki, Temperature effects on hyperon superfluids in neutron stars, *Nucl. Phys. A* **721**, C1003 (2003).
- [27] R. Xu, C. Wu, and Z. Ren, Superfluidity of Λ hyperons in warm strange hadronic star matter, *Int. J. Mod. Phys. E* **23**, 1450078 (2014).
- [28] T. Tanigawa, M. Matsuzaki, and S. Chiba, Possibility of $\Lambda\Lambda$ pairing and its dependence on background density in a relativistic Hartree-Bogoliubov model, *Phys. Rev. C* **68**, 015801 (2003).
- [29] T. Takatsuka, S. Nishizaki, Y. Yamamoto, and R. Tamagaki, Occurrence of hyperon superfluidity in neutron star cores, *Prog. Theor. Phys.* **115**, 355 (2006).
- [30] Y. N. Wang and H. Shen, Superfluidity of Λ hyperons in neutron stars, *Phys. Rev. C* **81**, 025801 (2010).
- [31] X. Yan, L. Guang-Zhou, W. Hong-Yan, D. Wen-Bo, and Z. En-Guang, Influence of σ^* and φ mesons on Λ hyperon 1S_0 superfluidity in neutron star matter, *Chin. Phys. Lett.* **29**, 059701 (2012).
- [32] J. Hu, Z. Zhang, S. Bao, and H. Shen, Phase transition in hot Λ hypernuclei within the relativistic Thomas-Fermi approximation, *Phys. Rev. C* **94**, 054325 (2016).
- [33] N. Guleria, S. K. Dhiman, and R. Shyam, A study of Λ hypernuclei within the Skyrme–Hartree–Fock model, *Nucl. Phys. A* **886**, 71 (2012).
- [34] X.-R. Zhou, E. Hiyama, and H. Sagawa, Exotic structure of medium-heavy hypernuclei in the Skyrme Hartree-Fock model, *Phys. Rev. C* **94**, 024331 (2016).
- [35] H.-T. Xue, Y.-F. Chen, Q. B. Chen, Y. A. Luo, H.-J. Schulze, and X.-R. Zhou, Deformation and spin-orbit splitting of Λ hypernuclei in the Skyrme-Hartree-Fock approach, *Phys. Rev. C* **107**, 044317 (2023).
- [36] C. Samanta, P. R. Chowdhury, and D. N. Basu, Lambda hyperonic effect on the normal drip lines, *J. Phys. G: Nucl. Part. Phys.* **35**, 065101 (2008).
- [37] C. Samanta, Generalized mass formula for non-strange, strange and multiply-strange nuclear systems, *J. Phys. G: Nucl. Part. Phys.* **37**, 075104 (2010).
- [38] J.-W. Cui, X.-R. Zhou, L.-X. Guo, and H.-J. Schulze, Investigation of single- and double- Λ hypernuclei using a beyond-mean-field approach, *Phys. Rev. C* **95**, 024323 (2017).
- [39] W.-Y. Li, J.-W. Cui, and X.-R. Zhou, Structure of $^9_{\Lambda}$ Be and $^{10}_{\Lambda\Lambda}$ Be using the beyond-mean-field Skyrme-Hartree-Fock approach, *Phys. Rev. C* **97**, 034302 (2018).
- [40] X. Y. Wu, H. Mei, J. M. Yao, and X.-R. Zhou, Beyond-mean-field study of the hyperon impurity effect in hypernuclei with shape coexistence, *Phys. Rev. C* **95**, 034309 (2017).
- [41] H. Güven, K. Bozkurt, E. Khan, and J. Margueron, $\Lambda\Lambda$ pairing in multistrange hypernuclei, *Phys. Rev. C* **98**, 014318 (2018).
- [42] Y.-T. Rong, P. Zhao, and S.-G. Zhou, Strength of pairing interaction for hyperons in multistrangeness hypernuclei, *Phys. Lett. B* **807**, 135533 (2020).
- [43] J. Guo, C. F. Chen, X.-R. Zhou, Q. B. Chen, and H.-J. Schulze, $\Lambda\Lambda$ pairing effects in spherical and deformed multi- Λ hyperisotopes, *Phys. Rev. C* **105**, 034322 (2022).
- [44] A. L. Goodman, Finite-temperature HFB theory, *Nucl. Phys. A* **352**, 30 (1981).
- [45] J. Cugnon, A. Lejeune, and H.-J. Schulze, Hypernuclei in the Skyrme-Hartree-Fock formalism with a microscopic hyperon-nucleon force, *Phys. Rev. C* **62**, 064308 (2000).
- [46] I. Vidaña, A. Polls, A. Ramos, and H.-J. Schulze, Hypernuclear structure with the new Nijmegen potentials, *Phys. Rev. C* **64**, 044301 (2001).
- [47] J. Margueron, E. Khan, and F. Gulminelli, Density functional approach for multistrange hypernuclei: Competition between Λ and $\Xi^{0,-}$ hyperons, *Phys. Rev. C* **96**, 054317 (2017).
- [48] N. Sandulescu, Nuclear superfluidity and specific heat in the inner crust of neutron stars, *Phys. Rev. C* **70**, 025801 (2004).
- [49] E. Chabanat, P. Bonche, P. Haensel, J. Meyer, and R. Schaeffer, A Skyrme parametrization from subnuclear to neutron star densities. Part II. Nuclei far from stabilities, *Nucl. Phys. A* **635**, 231 (1998).
- [50] P. Finelli, N. Kaiser, D. Vretenar, and W. Weise, In-medium chiral $SU(3)$ dynamics and hypernuclear structure, *Phys. Lett. B* **658**, 90 (2007).
- [51] J. Margueron and E. Khan, Suppression, persistence, and reentrance of superfluidity near and beyond the neutron drip, *Phys. Rev. C* **86**, 065801 (2012).
- [52] M. Belabbas, J. J. Li, and J. Margueron, Finite-temperature pairing re-entrance in the drip-line nucleus ^{48}Ni , *Phys. Rev. C* **96**, 024304 (2017).